RSC Advances

PAPER

View Article Online
View Journal | View Issue

Cite this: *RSC Adv.*, 2022, **12**, 4939

High-performance ReS_2 photodetectors enhanced by a ferroelectric field and strain field

Xiaochi Tai,[ab] Yan Chen, *[ac] Shuaiqin Wu,[a] Hanxue Jiao,[a] Zhuangzhuang Cui,[a] Dongyang Zhao,[ac] Xinning Huang,[a] Qianru Zhao,[a] Xudong Wang,[a] Tie Lin,*[a] Hong Shen, *[a] Xiangjian Meng,[a] Jianlu Wang[a] and Junhao Chu[ab]

Flexible optoelectronic devices have numerous applications in personal wearable devices, bionic detectors, and other systems. There is an urgent need for functional materials with appealing electrical and optoelectronic properties, stretchable electrodes with outstanding mechanical flexibility, and gate medium with flexibility and low power consumption. Two-dimensional transition metal dichalcogenides (TMDCs), a novel kind of widely studied optoelectrical material, have good flexibility for their ultrathin nature. P(VDF-TrFE) is a kind of organic material with good flexibility which has been proved to be a well-performing ferroelectric gate material for photodetectors. Herein, we directly fabricated a well-performing photodetector based on ReS_2 and P(VDF-TrFE) on a flexible substrate. The device achieved a high responsivity of 11.3 A W^{-1} and a high detectivity of 1.7 $\times$ 10^{10} Jones from visible to near-infrared. Moreover, with strain modulation, the device's responsivity improved 2.6 times, while the detectivity improved 1.8 times. This research provides a prospect of flexible photodetectors in the near-infrared wavelength.

Received 29th November 2021
Accepted 16th January 2022

DOI: 10.1039/d1ra08718e

rsc.li/rsc-advances

Introduction

During the past decade, two-dimensional (2D) transition metal dichalcogenides (TMDCs) have been widely studied owing to their unique properties, such as sizable bandgap,[1,2] optimal detection,[3,4] and ideal flexibility.[5–7] While most people focus on group-6 TMDCs (MoS_2, WS_2, $MoTe_2$, *etc.*),[8] a newly emerging group-7 TMDC material, ReS_2, has attracted much attention due to its unique thickness-independent direct band-gap ($E_g \approx 1.4$ eV).[9,10] Due to its unique 1T distorted structure, the interlayer coupling energy of ReS_2 is much weaker than other TMDCs.[9] The weak inter-layer coupling results in a continuous direct bandgap from bulk to monolayer, and the PL peak moves slightly (between 1.5 and 1.6 eV) with the intensity reduced. These properties made ReS_2 and its heterostructures[11–13] exhibit high performance in photodetectors. In addition, ReS_2 and its heterostructures exhibit polarization-dependent photoresponse.[14–16] To date, ReS_2-based field effect transistors have been reported to have a switching ratio as high as 10^7,[17] good detection performance (the photoresponsivity can reach up to 10^6 A W^{-1}),[18] and high response time up to 20 μs.[19] However, in those traditional photodetectors, a constant high gate voltage (V_g) and a large drain-source current (I_d) are applied to achieve good performance, which means high power consumption. Besides, the above devices used rigid dielectrics like oxides (Al_2O_3, SiO_2, *etc.*). As a result, the device structures and constructed materials heavily limit practical applications in flexible photoelectric devices, such as artificial electronic skin,[20] wearable systems,[5] bionic detectors,[21] *etc.* New dielectrics materials and new device structures are needed for further investigation to realize high-performance flexible devices.

Organic ferroelectric material P(VDF-TrFE) is a promising option for gate dielectrics. Ferroelectric materials, such as α-In_2Se_3,[22] $LiNbO_3$,[23] HfO_2 (ref. 24) *etc.*, has been proved to have good performance in ferroelectric field effect transistors (FeFETs). As to photodetectors, the ferroelectric field could increase the mobility, photoresponsivity, detectivity, and photoresponse speed.[25] Moreover, after polarization, the remanent polarization is strong enough to keep the device working for months, which means low power consumption.[26–28] On the other hand, as a solution-made organic material, it has huge potential for large-area flexible electronics. Previous researchers have made many nonvolatile memory devices[29,30] and capacitors[31–33] on flexible substrates to study the ferroelectric properties under strain.[34,35] However, the electrical and photoelectrical properties of 2D materials & P(VDF-TrFE) based FeFET under strain have not been studied. Thus, a study on high-performance flexible photodetectors enhanced by ferroelectric field and strain field is necessary.

[a]*State Key Laboratory of Infrared Physics, Shanghai Institute of Technical Physics, Chinese Academy of Sciences, 500 Yu Tian Road, Shanghai 200083, China. E-mail: lin_tie@mail.sitp.ac.cn; hongshen@mail.sitp.ac.cn*

[b]*School of Physical Science and Technology, ShanghaiTech University, Shanghai 201210, China*

[c]*Department of Materials, School of Physics and Electronic Science, East China Normal University, Shanghai 200241, China. E-mail: yanchen@ee.ecnu.edu.cn*

In this work, we fabricated a flexible ReS_2/P(VDF-TrFE) hybrid photodetector on a polyimide (PI) substrate and investigated its detection performance in tensile condition. The electric and optoelectronic properties are studied under ferroelectric field. When the incident wavelength is 830 nm, the device with ferroelectric top gate on PI substrate exhibits a responsivity of 11.3 A W^{-1}, and a detectivity of 1.7×10^{10} Jones without constant gate voltage. The response time reaches 6.1 ms. Under strain modulation, 2.6 times the responsivity of that without bending is achieved. When the device is released, the performance comes back to the initial level.

Experimental

Fig. 1(a) and (b) is the structure schematic and the optical microscope photograph of the ReS_2 photodetector, respectively. The few-layer ReS_2 nanosheets were mechanically exfoliated from bulk ReS_2 crystals (bought from Graphene) with an adhesive tape (Nitto tape) subsequently exfoliated with a polydimethylsiloxane (PDMS, Gelfilm from Gelpak) stamp. Several flakes with different thicknesses remain to adhere to the stamp and several flakes were transferred on the polyimide substrate. The regular-shaped flakes without wrinkles and cracks were chosen to form devices. This guaranteed strain applied evenly on devices. Next, the source (S) and drain (D) metal electrodes were fabricated using electron-beam lithography, thermal evaporation of Cr/Au films (15 nm/45 nm), and lift-off by acetone. The following step was coating the P(VDF-TrFE) (70 : 30 in mol%) film as the top gate material. Finally, the ultrathin semitransparent aluminum ($\approx$10 nm) electrodes were deposited. The thickness of ReS_2 is further confirmed by atomic force microscopy (AFM). As shown in Fig. 1(b), the thickness of ReS_2 is approximately 10 nm.

Here we chose PI as the substrate for its heat stability ranging from −200 to 300 °C, poison-free, and insoluble in organic solvents. This means compatible with silicon processes and suitable for most situations. PI material and 2D materials have a good affinity, so that 2D materials are easy to adhere to the PI substrate. PI is suitable for bending for its elasticity modulus is up to 3–4 GPa. In addition, the 25 μm-thickness polyimide is suitable for control, because 2D materials on thick polyimide are hard to be bent and 2D materials on thin polyimide are easy to have wrinkles.

ReS_2 flakes were analyzed *via* photoluminescence (PL) and Raman, which suggested the good quality of the multi-flakes as shown in Fig. 1(c) and (d). The PL peak obtained at ~1.5 eV indicates the multi-layer nature of ReS_2 showed in Fig. 1(c). In Fig. 1(d), we labeled two low frequencies A_g-like modes (located

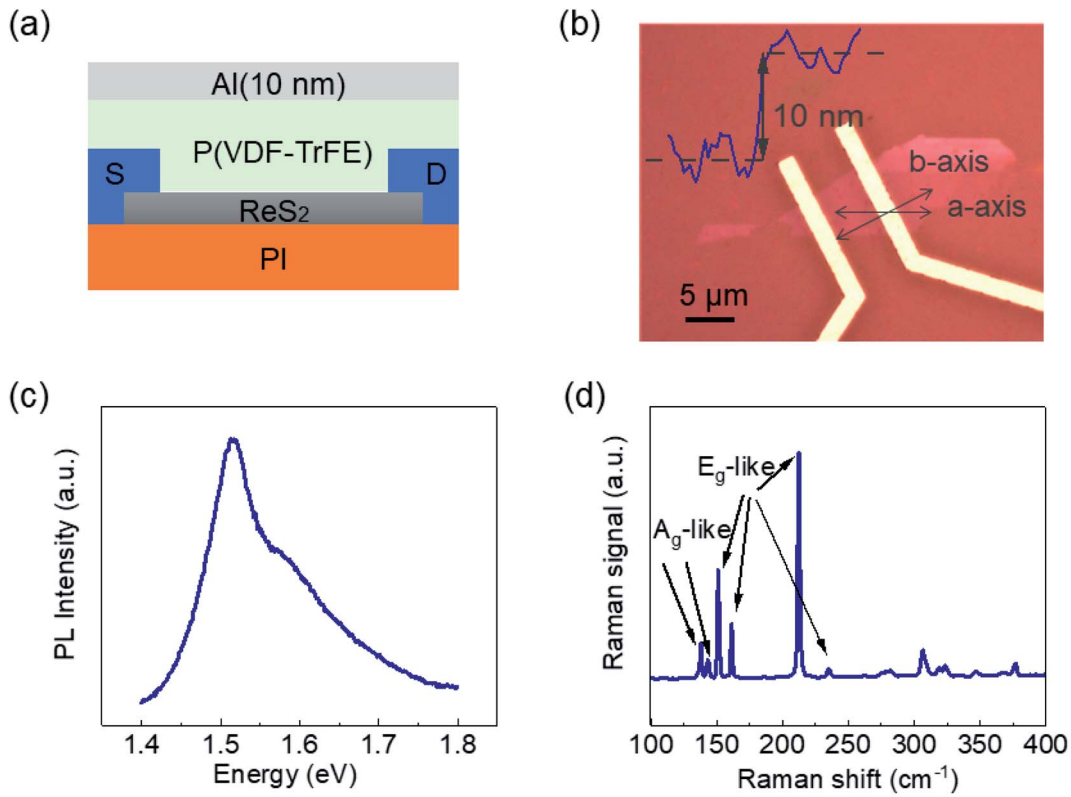

Fig. 1 Device structure and characteristics of ReS_2. (a) Schematic structure diagram of the ReS_2 photodetector on polyimide. The device is comprised of multi-layer ReS_2 with Cr/Au contract, 300 nm P(VDF-TrFE) ferroelectric polymer, and semitransparent aluminum top electrode (b) optical microscope photograph of the device with ReS_2 channel length of 5 μm, width of 4 μm. Scale bar, 5 μm. The inset is the AFM morphology of the device. (c) PL spectrum of the ReS_2 flake showing an optical band gap of ~1.5 eV. (d) Raman spectrum of the ReS_2 flake. Two low frequency A_g-like modes corresponding to the out-of-plane vibrations of Re atoms and four E_g-like modes corresponding to the in-plane vibrations of Re atoms. The rest 12 higher frequency Raman modes are vibrations mainly from lighter S atoms (the laser excitation wavelength is 532 nm).

at 136.8 and 144.5 cm^{-1}) corresponding to the out-of-plane vibrations of Re atoms and four E_g-like modes (located at 153.6, 163.4, 218.2, and 238.1 cm^{-1}) corresponding to the in-plane vibrations of Re atoms. The rest 12 higher frequency Raman modes are vibrations mainly from lighter S atoms.[36] This indicates that the ReS_2 used in this study is a multi-layer sample.

Results and discussion

First, we studied how the remnant polarization enhances the device's electric properties. The thickness of the P(VDF-TrFE) layer is 300 nm (measured by Step Profiler). The transfer curves (I_d–V_g) (drain-source current I_d as a function of top gate voltage V_g) of the ReS_2 transistor were tested at room temperature (shown in Fig. 2(a)). The large memory window ($\approx$25 V) in transfer curves between the voltage rise and decrease is related to the ferroelectric polarization switching process. The mobility $\mu \approx 115.3\ cm^2\ V^{-1}\ s^{-1}$ was calculated by

$$\mu = \frac{dI_d}{dV_g} \times \left(\frac{L}{(W\varepsilon_0\varepsilon_r/dV_d)} \right)$$

where $L = 5.0$ μm is the channel length, $W = 2.0$ μm is the channel width, $\varepsilon_r = 10$ is the dielectric constant of P(VDF-TrFE), $d = 300$ nm is the thickness of P(VDF-TrFE) films, and dI_d/dV_g is extracted from the left side of the transfer curve in Fig. 2(a). The output characteristic curves I_d–V_d of three different polarized states are showed in Fig. 2(b). The initial state of the P(VDF-TrFE) film is called fresh state. In this state, P(VDF-TrFE) film has not been polarized, and its dipoles are in disorder. No residual polarized electric field is generated, so it has little effect on the channel. A −40 V gate voltage applied made P(VDF-TrFE) film in polarization up state (P-up). The positive charges gather on the interface between P(VDF-TrFE) and ReS_2. These positive charges would deplete the charges in channel. Then the carrier concentration is reduced and the dark current could be so low. Besides, the increase of the barrier also reduces the dark current. A 40 V gate voltage applied made P(VDF-TrFE) film in polarization down state (P-down). The negative charges gather on the interface and the channel was fully accumulated. Current in P-up state is five orders of magnitude smaller than current in P-down state. Operating the device in the P-up state brings the advantage of a reduced dark current.

Next, the photoresponse of the ReS_2 photodetector was measured at a ZERO gate voltage in the P-up state. As is shown in Fig. 3(a), the light at 830 nm is incident perpendicularly to the device surface, and the spot covers the entire channel uniformly. The ultrahigh local electrostatic field induced by the upward-polarized P(VDF-TrFE) makes the ReS_2 channel fully depleted, which means the photodetector would have an ultra-low dark current. As a result, the ferroelectric field keeps the ReS_2 photodetector at a sensitive state in a power efficient way. The photo switching properties (under $V_d = 100$ mV) at a wavelength of 830 nm and 1310 nm are shown in Fig. 3(b). The detector has good response for the wavelength of 830 nm light illumination and almost no response for 1310 nm. Fig. 3(c) shows the photocurrent exhibits rapid rise/fall and reaches a steady saturation. The rise (t_r) and decay (t_f) times of photocurrent are measured as 6.6 ms and 6.1 ms, respectively, and both the rise and decay curves (in black) are fitted well using a single exponential functions (in red) shown in Fig. 3(c). The responsivity $R = I_{ph}/P_{eff}$, where I_{ph} is the photocurrent in a detector and P_{eff} is the effective illumination power. It is worth mentioning that P_{eff} is calculated by $P_{eff} = AP\pi^{-1}r^{-2}$, where A is the area of the sample, P is the actual laser output and r is the radius of the laser spot size. In addition, the detectivity, assuming that noise from dark current is the major factor, is given by $D^* = RA^{1/2}/(2eI_{dark})^{1/2}$, where R is the responsivity, A is the area of the detector, e is the unit charge, and I_{dark} is the dark current (under 0.1 V bias here).[24,37] The device exhibits a photoresponsivity (R) of 11.3 A W^{-1}, and the detectivity (D^*) is up to 1.7×10^{10} Jones approximately when the wavelength is 830 nm, a laser power of 1 pW, and $V_d = 100$ mV. The maximum detectivity of 1.7×10^{10} Jones has been achieved. As shown in Fig. 3(d), the high detectivity and responsivity decrease dramatically with the increasing signal power.

Based on the research of P(VDF-TrFE) based FeFET, the photoelectric properties under strain are studied. To apply

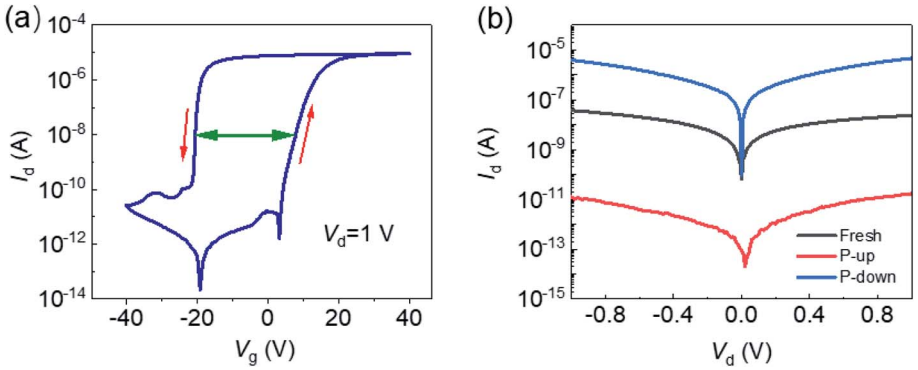

Fig. 2 Electric properties of the P(VDF-TrFE)/ReS_2 FET without deformation. (a) The transfer curves of multilayer ReS_2 channel with P(VDF-TrFE) ferroelectric polymer gate on dark state at room temperature. (b) The V_d–I_d characteristics (at ZERO gate voltage) with three states of the ferroelectric layer. The three states are: fresh state (ferroelectric layer without polarization), polarization up ("P-up" polarized by a pulse V_g of −40 V), and polarization down ("P-down" polarized by a pulse V_g of −40 V) states, respectively.

strain on the devices, we made several half-cylinders printed by a 3D printer, then fixed the polyimide substrate on the curved surfaces (shown in Fig. 4(a)). The strains were quantified by the equation: $\varepsilon = (t/r)/2$,[6] where t is the substrate thickness (25 μm for the PI substrates used here) and r is the bending radius of 30, 15, 10, 5 mm. Assuming that as-fabricated exfoliated devices before bending are virtually strain-free,[38] we get five strains $\varepsilon \approx$ 0.00, 0.04, 0.08, 0.125, and 0.25%, respectively. The channel is along the *b*-axis (as shown in Fig. 1(b)), and so is the strain. This is the optimal option for strain modulation in this study. Fig. 4(b) shows the output characteristics of FeFET under different strains in dark state. The dark current went through a decrease under little strain and an increase when strain becomes larger. The '0' state is the state before bending and after polarization. The '0-again' state is the state return to '0' state after bending. Fig. 4(c) shows the normalized photoresponsivity of the ReS_2 phototransistor under strain. When a little strain is applied, the responsivity increases with the increase of strain. When the strain is 0.08%, the optical response reaches a maximum which is 2.6 times that strain is 0. The responsivity keeps a steady level when the strain is over 0.08%. Fig. 4(d) shows the normalized detectivity of the ReS_2 phototransistor under strain. When the strain is 0.08%, the optical response reaches its maximum, which is 1.8 times that strain is 0. This means the device can achieve the best photoresponse with the 0.08% strain applied where the minimum dark current achieved. In addition, when the device was released, it was almost returned to its original state, and the process can be repeated.

Fig. 4(e)–(g) show the mechanism of strain modulation of the photodetector. The top electrode, P(VDF-TrFE) and ReS_2 could be seen as a parallel plate capacitor. In a parallel plate capacitor, total quantity of electric charge (Q) is defined as $Q = \varepsilon_0\varepsilon_r SE$, where ε_0 is the permittivity of vacuum, ε_r is the relative permittivity, S is the area of plate and E is the electric field intensity. When a small strain applied, the electric field (E) provided by P(VDF-TrFE) is constant whereas the area (S) increases. This would lead to the increase of quantity of electric charge (Q). The increasing of Q at the interface between P(VDF-TrFE) and ReS_2 would get more charges depleted. Thus, the carrier concentration reduces and the Fermi energy raises up. The dark current becomes lower then. With strain increase further, the dark current increases. The increase of dark current is mainly due to the narrowing of ReS_2' bandgap. When the channel direction was made along the *b*-axis and the strain was applied along the channel direction, the decrease of the VBM is slower than that of the CBM, leading to the narrowing of the bandgap.[36] As the carriers are fully depleted in P-up state, $E_c - E_F = E_g/2$, where E_c is the conduction band edge, E_F is the Fermi energy and E_g is the bandgap. The conductivity of the semiconductor is expressed as

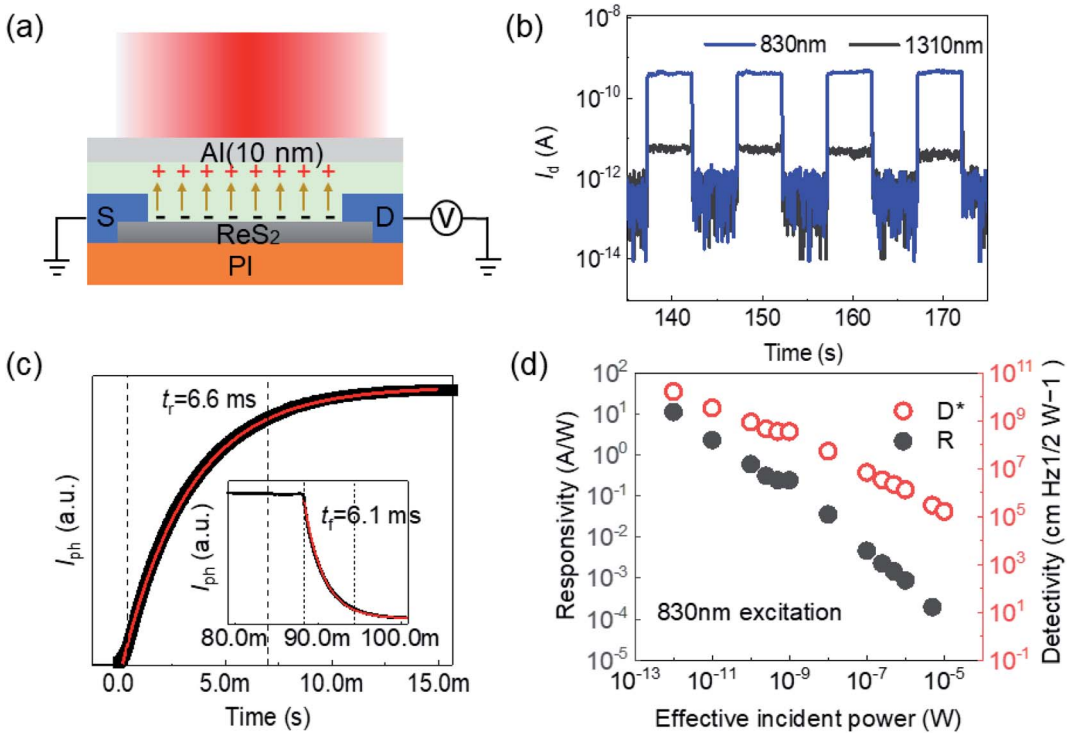

Fig. 3 Optoelectronic properties of the P(VDF-TrFE)/ReS_2 FET on PI substrates without deformation. (a) Laser is incident perpendicularly to the device surface, and the spot covers the entire channel uniformly. (b) Photoswitching behavior of the photodetector without ferroelectric polarization gate and in the P_{up} state, respectively (λ = 830 nm and 1310 nm, V_d = 100 mV, P_{eff} = 1 nW). (c) The rise and fall of the photocurrent and the fitted data using exponential functions (recorded by V_d = 100 mV and P_{eff} = 1 nW). (d) Photoresponsivity of the ReS_2 phototransistor, showing high sensitivity. The device exhibits a photoresponsivity (R) of 11.3 A W^{-1}, and the detectivity (D^*) is up to ≈1.7 × 10^{10} Jones when the wavelength is 830 nm and a laser power of 1 pW.

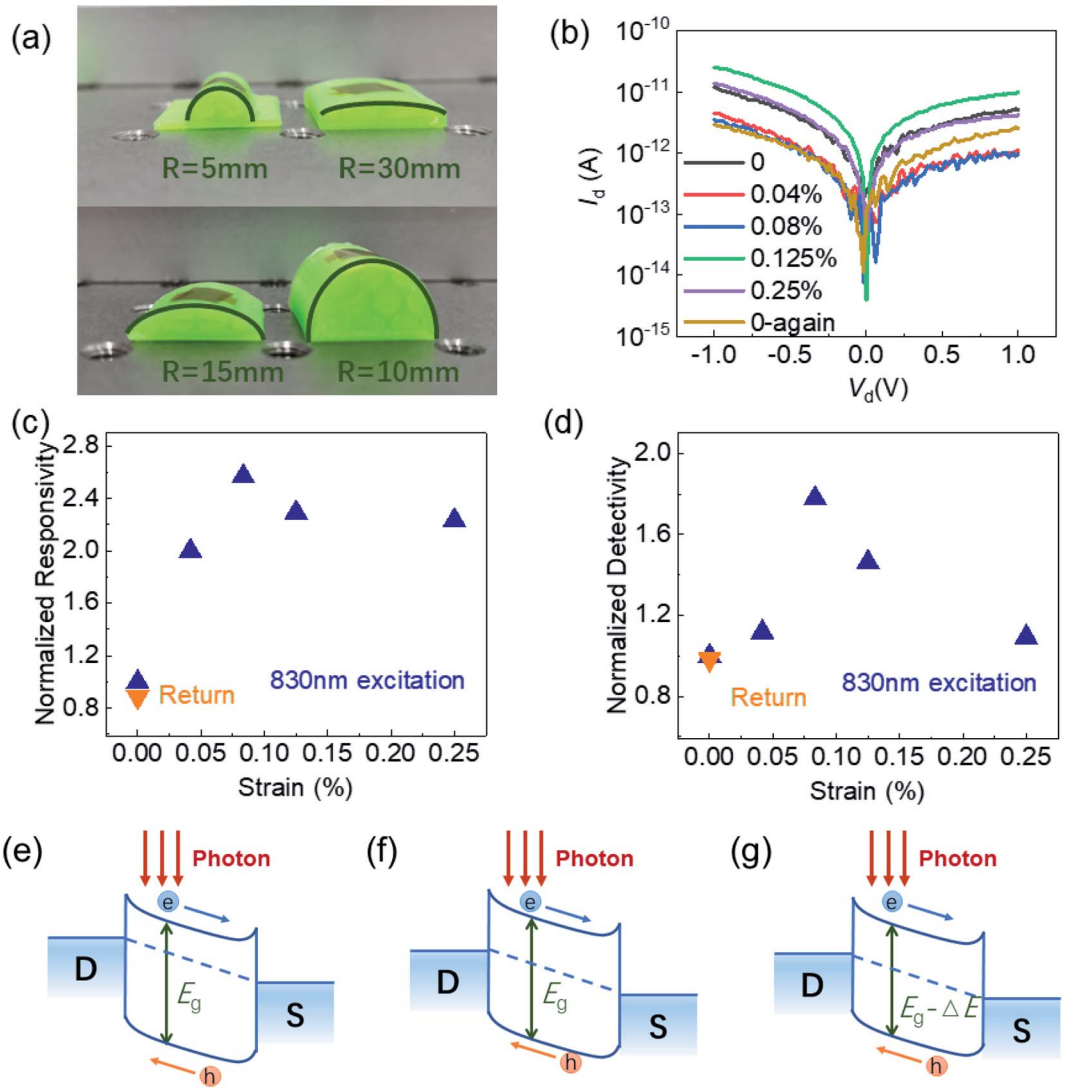

Fig. 4 Photoresponse properties of the ferroelectric polarization gating multi-layer ReS_2 photodetector under deformation. (a) Optical imagine and schematic diagram of the bent installation. The curved models with radius of 30 mm, 15 mm, 10 mm and 5 mm are printed by Flash Forge Creator Pro. The device on polyimide then is closely fixed on the top of the model. (b) The dark currents of the ReS_2 phototransistor under different strains. The '0' state is the state before bending and after polarization. The '0-again' state is the state return to '0' state after bending. (c) Normalized photoresponsivity of the ReS_2 phototransistor under strain. (d) Normalized detectivity of the ReS_2 phototransistor under strain. The orange point is the value after bending and the strain is released. (e and f) The energy band diagrams under (e) no strain, (f) little strain, (g) larger strain with $V_{sd} = 0.1$ V, the symbols "e" (in blue) and "h" (in orange) represent the electrons and holes excited by the incident photon. E_g represents the bandgap of ReS_2.

$$\sigma = \sigma_0 \exp\left[-\frac{E_c - E_F}{k_B T}\right] = \sigma_0 \exp\left[-\frac{E_g}{2k_B T}\right],$$

where, σ_0 is the minimum conductivity defined by the hopping distance, k_B is the Boltzmann constant and T is temperature. Therefore, the conductivity would increase with the bandgap decreasing. For the dark current is proportional to σ, the dark current increases. Besides, it was witnessed that the dark current after bending released is smaller than the dark current before bending. That results from some charged interface states disappearing after bending. Based on the modulation on dark current, the corresponding responsivity and detectivity were modulated accordingly. Overall, the performance of the photodetector is further enhanced by strain modulation.

Conclusions

In conclusion, we have fabricated a ferroelectric polymer film gated multi-layer ReS_2 phototransistor on flexible polyimide. The electronic and optoelectronic properties of the device on the flexible substrate were systematically studied. As a result, the device on PI substrate with ferroelectric top gate exhibits a maximum attainable responsivity of 11.3 A W^{-1}, and the detectivity of 1.7×10^{10} Jones when the wavelength is 830 nm without gate voltage. Then, we bent the device to modulate the responsivity and get 2.6 times responsivity and 1.8 times detectivity enhancement. It will be a great gain for a photodetector array.[39] This flexible device promises potential in wearable installation, bionic detectors, biomedical systems, *etc.*

Author contributions

X. T. and X. H. fabricated devices. H. J. and S. W. guided the device fabrication. Y. C. and H. S. conceived the idea for the project and designed the experiments. X. T., S. W. and T. L. performed the electronic and optoelectronic measurements. X. W., Y. C., S. W., T. L., H. S., W. H., X. M. and J. W. analyzed the data. X. T. and Y. C. wrote the manuscript. All the authors discussed the results and commented on the manuscript.

Conflicts of interest

The authors declare no conflict of interest.

Acknowledgements

This work is supported by Natural Science Foundation of China (Grant No. 62025405, 61905267, 61835012, 62075228, 61974153 and 62004204), Strategic Priority Research Program of the Chinese Academy of Sciences (Grant No. XDB44000000), the Key Research Project of Frontier Sciences of Chinese Academy of Sciences (QYZDY-SSW-JSC042), the Key Research Program of Frontier Sciences, CAS (Grant No. ZDBS-LY-JSC045), Shanghai Sailing Program (Grant No. 19YF1454900, 21YF1454800), China Postdoctoral Science Foundation (Grant No. 2019M661431, 2020M671245), and the Russian Foundation for Basic Researches (RFBR) (Grant No. 19-01-00519, 20-51-53014 and 62011530043).

References

1 J. A. Wilson and A. D. Yoffe, *Adv. Phys.*, 1969, **18**(73), 193.
2 A. D. Yoffe, *Annu. Rev. Mater. Sci.*, 1973, **3**(1), 147.
3 B. Radisavljevic, A. Radenovic, J. Brivio, V. Giacometti and A. Kis, *Nat. Nanotechnol.*, 2011, **6**(3), 147.
4 Q. H. Wang, K. Kalantar-Zadeh, A. Kis, J. N. Coleman and M. S. Strano, *Nat. Nanotechnol.*, 2012, **7**(11), 699.
5 D. Akinwande, N. Petrone and J. Hone, *Nat. Commun.*, 2014, **5**, 5678.
6 H. J. Conley, B. Wang, J. I. Ziegler, R. F. Haglund Jr, S. T. Pantelides and K. I. Bolotin, *Nano Lett.*, 2013, **13**(8), 3626.
7 M. Y. Tsai, A. Tarasov, Z. R. Hesabi, H. Taghinejad, P. M. Campbell, C. A. Joiner, A. Adibi and E. M. Vogel, *ACS Appl. Mater. Interfaces*, 2015, **7**(23), 12850.
8 K. Thakar and S. Lodha, *Mater. Res. Express*, 2020, **7**(1), 014002.
9 S. Tongay, H. Sahin, C. Ko, A. Luce, W. Fan, K. Liu, J. Zhou, Y. S. Huang, C. H. Ho, J. Y. Yan, D. F. Ogletree, S. Aloni, J. Ji, S. S. Li, J. B. Li, F. M. Peeters and J. Q. Wu, *Nat. Commun.*, 2014, **5**, 3252.
10 E. Liu, Y. Fu, Y. Wang, Y. Feng, H. Liu, X. Wan, W. Zhou, B. Wang, L. Shao, C. H. Ho, Y. S. Huang, Z. Cao, L. Wang, A. Li, J. Zeng, F. Song, X. Wang, Y. Shi, H. Yuan, H. Y. Hwang, Y. Cui, F. Miao and D. Xing, *Nat. Commun.*, 2015, **6**, 6991.
11 A. Varghese, D. Saha, K. Thakar, V. Jindal, S. Ghosh, N. V. Medhekar, S. Ghosh and S. Lodha, *Nano Lett.*, 2020, **20**(3), 1707.
12 S.-H. Jo, H. W. Lee, J. Shim, K. Heo, M. Kim, Y. J. Song and J.-H. Park, *Adv. Sci.*, 2018, **5**(4), 1700423.
13 A.-J. Cho, S. D. Namgung, H. Kim and J.-Y. Kwon, *APL Mater.*, 2017, **5**(7), 076101.
14 W. Zhu, W. Xia, F. Yan, Q. Lv, C. Hu and K. Wang, *J. Semicond.*, 2019, **40**, 092001.
15 F. Liu, S. Zheng, X. He, A. Chaturvedi, J. He, W. L. Chow, T. R. Mion, X. Wang, J. Zhou, Q. Fu, H. J. Fan, B. K. Tay, L. Song, R.-H. He, C. Kloc, P. M. Ajayan and Z. Liu, *Adv. Funct. Mater.*, 2016, **26**(8), 1169.
16 D. Liu, J. Hong, X. Wang, X. Li, Q. Feng, C. Tan, T. Zhai, F. Ding, H. Peng and H. Xu, *Adv. Funct. Mater.*, 2018, **28**(47), 1804696.
17 E. Liu, M. Long, J. Zeng, W. Luo, Y. Wang, Y. Pan, W. Zhou, B. Wang, W. Hu, Z. Ni, Y. You, X. Zhang, S. Qin, Y. Shi, K. Watanabe, T. Taniguchi, H. Yuan, H. Y. Hwang, Y. Cui, F. Miao and D. Xing, *Adv. Funct. Mater.*, 2016, **26**(12), 1938.
18 L. C. Jing Xu, Y. W. Dai, Q. Cao, Q.-Q. Sun, S. J. Ding, H. Zhu and D. W. Zhang, *Sci. Adv.*, 2017, **3**, 1602246.
19 K. Thakar, B. Mukherjee, S. Grover, N. Kaushik, M. Deshmukh and S. Lodha, *ACS Appl. Mater. Interfaces*, 2018, **10**(42), 36512.
20 D. H. Kim, N. Lu, R. Ma, Y.-S. Kim, R. H. Kim, S. Wang, J. Wu, S. M. Won, H. Tao, A. Islam, K. J. Yu, T. i. Kim, R. Chowdhury, M. Ying, L. Xu, M. Li, H. J. Chung, H. Keum, M. McCormick, P. Liu, Y. W. Zhang, F. G. Omenetto, Y. Huang, T. Coleman and J. A. Rogers, *Science*, 2011, **333**, 838.
21 J. A. Rogers, T. Someya and Y. Huang, *Science*, 2010, **327**, 1603.
22 M. Si, A. K. Saha, S. Gao, G. Qiu, J. Qin, Y. Duan, J. Jian, C. Niu, H. Wang, W. Wu, S. K. Gupta and P. D. Ye, *Nat. Electron.*, 2019, **2**(12), 580.
23 L. Tong, Z. Peng, R. Lin, Z. Li, Y. Wang, X. Huang, K.-H. Xue, H. Xu, F. Liu, H. Xia, P. Wang, M. Xu, W. Xiong, W. Hu, J. Xu, X. Zhang, L. Ye and X. Miao, *Science*, 2021, **373**(6561), 1353.
24 L. Tu, R. Cao, X. Wang, Y. Chen, S. Wu, F. Wang, Z. Wang, H. Shen, T. Lin, P. Zhou, X. Meng, W. Hu, Q. Liu, J. Wang, M. Liu and J. Chu, *Nat. Commun.*, 2020, **11**(1), 101.
25 X. Wang, P. Wang, J. Wang, W. Hu, X. Zhou, N. Guo, H. Huang, S. Sun, H. Shen, T. Lin, M. Tang, L. Liao, A. Jiang, J. Sun, X. Meng, X. Chen, W. Lu and J. Chu, *Adv. Mater.*, 2015, **27**(42), 6575.
26 X. Wang, C. Liu, Y. Chen, G. Wu, X. Yan, H. Huang, P. Wang, B. Tian, Z. Hong, Y. Wang, S. Sun, H. Shen, T. Lin, W. Hu, M. Tang, P. Zhou, J. Wang, J. Sun, X. Meng, J. Chu and Z. Li, *2D Mater.*, 2017, **4**(2), 025036.
27 R. C. G. Naber, C. Tanase, P. W. M. Blom, G. H. Gelinck, A. W. Marsman, F. J. Touwslager, S. Setayesh and D. M. de Leeuw, *Nat. Mater.*, 2005, **4**(3), 243.
28 S. Z. Yuan, X. J. Meng, J. L. Sun, Y. F. Cui, J. L. Wang, L. Tian and J. H. Chu, *Phys. Lett. A*, 2011, **375**(14), 1612.
29 G. G. Lee, E. Tokumitsu, S. M. Yoon, Y. Fujisaki, J. W. Yoon and H. Ishiwara, *Appl. Phys. Lett.*, 2011, **99**(1), 012901.

30 S. M. Yoon, S. Yang, M. K. Ryu, C. W. Byun, S. W. Jung, S. H. K. Park, C. S. Hwang and K. I. Cho, *IEEE Trans. Electron Devices*, 2011, **58**(7), 2135.
31 Z. Pi, J. Zhang, C. Wen, Z. Zhang and D. Wu, *Nano Energy*, 2014, **7**, 33.
32 G. X. Ni, Y. Zheng, S. Bae, C. Y. Tan, O. Kahya, J. Wu, B. H. Hong, K. Yao and B. Özyilmaz, *ACS Nano*, 2012, **6**(5), 3935.
33 S. H. Bae, O. Kahya, B. K. Sharma, J. Kwon, H. J. Cho, B. Özyilmaz and J. H. Ahn, *ACS Nano*, 2013, **7**(4), 3130.
34 M. Guo, C. Guo, J. Han, S. Chen, S. He, T. Tang, Q. Li, J. Strzalka, J. Ma, D. Yi, K. Wang, B. Xu, P. Gao, H. Huang, L. Q. Chen, S. Zhang, Y. H. Lin, C. W. Nan and Y. Shen, *Science*, 2021, **371**(6533), 1050.
35 D. Singh, Deepak and A. Garg, *Phys. Chem. Chem. Phys.*, 2016, **18**(42), 29478.
36 Y. Feng, W. Zhou, Y. Wang, J. Zhou, E. Liu, Y. Fu, Z. Ni, X. Wu, H. Yuan, F. Miao, B. Wang, X. Wan and D. Xing, *Phys. Rev. B: Condens. Matter Mater. Phys.*, 2015, **92**(5), 054110.
37 M. Long, P. Wang, H. Fang and W. Hu, *Adv. Funct. Mater.*, 2019, **29**(19), 1803807.
38 C. Y. Chen, S. Rosenblatt, K. I. Bolotin, W. Kalb, P. Kim, I. Kymissis, H. L. Stormer, T. F. Heinz and J. Hone, *Nat. Nanotechnol.*, 2009, **4**(12), 861.
39 W. Wu, L. Wang, Y. Li, F. Zhang, L. Lin, S. Niu, D. Chenet, X. Zhang, Y. Hao, T. F. Heinz, J. Hone and Z. L. Wang, *Nature*, 2014, **514**(7523), 470.